N89-12915

ELEVATED TEMPERATURE CRACK GROWTH*

S.N. Malik, R.H. Van Stone, K.S. Kim, J.H. Laflen
General Electric Company

INTRODUCTION

Critical gas turbine engine hot section components such as blades, vanes, and combustor liners tend to develop minute cracks during the early stages of operation. These cracks may then grow under conditions of fatigue and creep to critical size. Current methods of predicting growth rates or critical crack sizes are inadequate, which leaves only two extreme courses of action. The first is to take an optimistic view with the attendant risk of an excessive number of service failures. The second is to take a pessimistic view and accept an excessive number of "rejections for cause" at considerable expense in parts and downtime. Clearly is is very desirable to develop reliable methods of predicting crack growth rates and critical crack sizes.

To develop such methods, it is necessary to relate the processes that control crack growth in the immediate vicinity of the crack tip to parameters that can be calculated from remote quantities, such as forces, stresses, or displacements. The most likely parameters appear to be certain path-independent (PI) integrals, several of which have already been proposed for application to high temperature inelastic problems. A thorough analytical and experimental evaluation of these parameters needs to be made which would include elevated temperature isothermal and thermo-mechanical fatigue, both with and without thermal gradients.

Investigations of fatigue crack growth under elastic-plastic condition should consider the impact of crack closure on the appropriate crack growth model. Analytically, this requires the use of gap elements in a nonlinear finite element code to predict closure loads. Such predictions must be verified experimentally through detailed measurements; the best method for measuring crack closure has not been established in previous studies.

It is the purpose of this contract (NAS3-23940) to determine the ability of currently available PI-integrals to correlate fatigue crack propagation under conditions that simulate the engine combustor liner environment. The utility of advanced fracture mechanics measurements will also be evaluated and determined during the course of the program. These goals are to be accomplished through a nine task, combined experimental and analytical program. To date, an appropriate specimen design, a crack displacement measurement method, and boundary

* Work done under NASA Contract NAS3-23940.

condition simulation in the computational model of the specimen has been achieved. Computational verification of the path-independence of the proposed integrals has been demonstrated for isothermal and thermal gradient cases. Also, the experimental testing and data acquisition is continuing. Tensile and cyclic tests were run at several strain-rates so that an appropriate constitutive model could be developed. The experimental data include cyclic crack growth tests under isothermal, thermo-mechanical, and thermal gradient conditions.

EXPERIMENTAL PROGRAM

Alloy 718, a γ-γ" nickel-base superalloy, has been selected as the analog material for this program because over the temperature range from 800 to 1200°F, it shows very large changes in creep behavior. This permits the use of Alloy 718 to simulate the behavior of combustor liner materials while still performing experiments at a relatively low temperature. Tensile, creep and cyclic constitutive tests have been performed over the temperature range from 70 to 1200°F. Even though this material can experience large amounts of creep deformation at the upper end of this temperature range, the tensile and cyclic tests showed little evidence of strain rate sensitivity on constitutive response. Figure 1 shows the resultant tensile stress strain curves determined for 70, 800, and 1200°F. Tensile curves were also determined at 900, 1000 and 1100°F. These curves were used during the analysis of the temperature gradient tests which are described later in this paper.

The crack growth tests have been performed using a single edge notch (SEN) specimen with buttonhead grips. The width and thickness of the gage section is 0.4 and 0.1 inch, respectively. Detailed descriptions of the specimen, testing procedure and finite element analyses have been described previously [1]. The SEN tests were performed in a strain control mode with the experimental setup shown schematically in Figure 2. The controlling extensometer was mounted at the center of the 0.4 inch wide surface of the specimen. The other two displacement gages, one to monitor crack mouth opening displacement and one to monitor the back face deflection, were also used. The controlling and back face extensometers had a gage length of 0.5 inch and the crack mouth gage had a gage length of 0.03 inch. The crack length was monitored using a DC potential drop technique. The hysteresis loops from these tests [1] were open, indicative of large net section non-linear deformation (i.e., plasticity and creep). Figure 3 shows the data from four 1000°F, $A_c=\infty$ crack growth rate tests - single tests at strain ranges of 0.5 and 1.7% and duplicate tests at 1.15% strain range. The initial EDM notch depth was approximately 0.01 inch. Figure 3a shows the strong influence of strain range on the crack growth behavior. The results from the duplicate 1.15% tests are very similar. During these strain control tests, the maximum loads diminished as the crack grew. Figures 3b and 3c show the 1000°F crack growth rates (da/dN) plotted as a function of ΔK and K_{max}, respectively. These data show that these tests cover a range of conditions which can not be described by K, which is proportional to the crack tip stress field in linear elastic fracture mechanics. Comparison of

Figures 3b and 3c also shows that the crack growth rates are better described by K_{max} than ΔK. This suggests that when the final analysis of these tests is completed, the adjustments for crack closure will describe the behavior over the entire range of crack length.

Thermal gradient tests have been performed to evaluate the PI-integrals under non-isothermal conditions. The thermal gradient was established using a combination of induction heating and forced air cooling. At the front or cracked surface, the crack mouth opening extensometer prevented the use of cooling air so the crack was grown from the high temperature to the low temperature. Cooling air was applied to the back face of the specimen above and below the extensometer with cooling tubes and to the gage section with air forced through the cooling passages in the extensometer probes. This gradient technique was originally developed on a specimen which was monitored with fifteen thermocouples. Three sets of five thermocouples were attached to the specimen along the crack plane and at planes 0.25 inch above and below the crack plane. The two latter locations correspond to the positions where the arms of the two large gage length extensometers contact the specimen. On all three planes, a thermocouple was located at each edge of the specimen and at four equally spaced intervals. The presence of the thermocouples prevented the attachment of the three extensometers, so the temperatures were monitored along the plane of the crack in another specimen using an optical pyrometer attached to a traveling microscope. The results of the temperature measurements are shown in the Figure 4. The line connecting the "X" symbols represent the optical pyrometry measurements. These results show a small amount of temperature difference from specimen-to-specimen and along the gage length. This variation is within an acceptable range.

COMPUTATIONAL PROGRAM

Major computational accomplishment was the implementation, verification, and applications of the selected PI-integrals to uniform and non-uniform thermal gradients, and thermo-mechanical loadings for fracture mechanics analyses involving nonlinear material stress/strain behavior. A critical review [2] of the available J_x-integrals conducted under this program revealed that PI-integrals proposed by Ainsworth (J_θ), Blackburn (J*), Kishimoto (J), and Atluri (T_p^* and T_p) are suitable for nonlinear thermo-mechanical response. The relative advantages and limitations of the various J_x-integrals for thermal gradient problems are discussed in-depth in Reference [2]. The traditional Rice J-integral becomes path-dependent and loses its physical significance for thermo-mechanical loadings due to presence of the mechanical (rather than total) strain energy in its formulation and, also, due to the absence of thermal strains contribution and non-homogeneous (temperature dependent) material properties.

Verification of the implemented thermo-mechanical J_x-integrals was carried out by prescribing a linear temperature gradient through the width of the SEN (single edge notch) crack specimen which was gradually loaded with far-field

uniform normal stress. The crack length to specimen width ratio (a/W) is 0.25 and the specimen length to width ratio (L/W) is 1.25. The specimen edge at crack face was kept at 1200°F temperature and the back-face edge had a temperature of 1000°F. All properties of the material were kept temperature dependent and, as such, they varied through the specimen width. Therefore, the material properties are non-homogeneous along the direction of thermal gradient.

Nonlinear, thermo-mechanical, finite element (FEM) analyses of the SEN specimen were carried out for several values of the applied uniform stress, resulting in thermo-elastic to thermo-elastic/plastic response. Figure 5 shows the far-field normal displacement (Uy) variation which is linear in nature through the specimen width for all the load cases considered. A significant amount of plastic yielding is taking place ahead of the crack for the larger values of the applied stress as seen in Figure 6 which shows the effective stress contours in the specimen. The FEM analyses results were then used in the post-processor PI-integral computer code to determine the various J_x-integrals for several integration paths around the crack tip. Table 1 shows a typical variation of the various J_x-integrals along four paths spanning extreme plasticity to pure elastic regions near the crack. It could be seen that the Rice J-integral values are path dependent for the thermo-mechanical load case. The other five J_x-integrals shown in Table 1 are path-independent. A few of these thermo-mechanical PI-integrals are plotted in Figure 7 for various applied normal stress values. These integrals show excellent agreement with isothermal Elastic-Plastic Fracture Mechanics (EPFM) Handbook [3] and Tada/Paris [4] analytical solutions for lower values of applied stresses. For higher values of applied stress, the thermo-mechanical PI-integrals attain larger values as compared to analytical isothermal J-integral. These results demonstrate implementation and verification of the thermo-mechanical PI-integrals considered here.

To minimize the finite boundary effects, the specimen L/W ratio used in verification analysis was 1.25. For the actual specimen, however, the L/W ratio is only 0.78. Therefore, in order to investigate the influence of finite boundary on J_x-integrals, the same linear thermal gradient analysis was carried for the actual specimen. Typical results as shown in Figure 8 indicate a maximum deviation of 3% on PI-integrals for the prescribed applied stresses.

The actual thermal gradient developed in the SEN specimen gage-section can be approximated as trilinear relationship, as shown in Figure 9. It is approximately constant at 1200°F for the first 0.175 inch along the specimen width; it then linearly drops to 1050°F for the next 0.14 inch of the width; and, finally, it varies linearly to 900°F in the remaining 0.08 inch of the width. Stress analysis of the specimen with the measured temperature dependent material properties and the prescribed trilinear thermal gradient was performed. An interesting result was observed for the pure thermal gradient load case (zero applied load/deflection). For an a/W ratio of 0.25, a crack mouth opening displacement of 0.00015 inch was predicted. The corresponding far-field normal displacement for pure thermal expansion load case is shown in Figure 10 for two

cross sections - one at y = 0.31 inch (end of gage length), and the other at y = 0.25 inch (location of extensometer probes). These free-thermal-expansion normal displacements vary nonlinearly, through the specimen width, due to a combination of the temperature dependent material properties and the trilinear thermal gradient. It has been shown previously that the far-field mechanical displacement in the specimen varies linearly along the specimen width at the end of gage-section. Figure 11 shows the normal stress variation ahead of the crack-tip for the pure thermal gradient load case. The normal stress has a value of 20 ksi near the crack-tip and it drops sharply to -8 ksi at x = 0.175 inch and then gradually increases to 12 ksi by the end of the specimen width. This normal thermal stress is self-equilibrating in nature since there is no mechanical load applied. This fact is further elaborated in Figure 12 which shows the contour plots of the normal stress in the entire gage-section of the specimen. It could be seen that at the top surface (end of the gage-length) the normal stress is zero along entire width of the specimen. The whole specimen is in elastic state of stress with a maximum effective stress of 35 ksi. Since there exists a crack-tip stress field in the specimen for the measured thermal gradient load case, the various J_x-integrals were determined and found to be path-independent. The average value of these PI-integrals was 1.16 lbs/inch, which is equivalent to 5 ksi$\sqrt{\text{in}}$ thermal-K_I value.

Stress analyses were further carried out by prescribing uniform normal stresses superimposed on the actual specimen with the measured thermal gradient. Figure 13 shows the variation of the thermo-mechanical J_x-integrals with applied stress. It could be seen that the values of these integrals are very close to each other for lower values of the applied stress with very little plasticity in the specimen. When the level of plasticity increases, then the various PI-integrals have somewhat different values but remain path-independent.

CONCLUDING REMARKS

The analyses conducted for thermo-mechanical PI-integrals have been very successful and compare very well with the available results. Work is now in progress for computational simulation of the measured load-displacement plots for the thermo-mechanical response of the specimen. In addition, computations are also to be performed for reversed plastic loading to simulate crack-closure. These results will be compared with crack growth experimental measurements to identify path-independent integrals which can predict cyclic crack growth behavior under isothermal, TMF, and thermo-mechanical loading conditions.

REFERENCES

1. Malik, S. N., Van Stone, R. H., Kim, K. S., and Laflen, J. H., "Elevated Temperature Crack Growth," pp. 329-340, NASA Conference Publication 2405, Turbine Engine Hot Section Technology Conference, NASA Cleveland, Oct. 1985.

2. Kim, K. S. and Orange, T. W., "A Review of Path-Independent Integrals in Elastic-Plastic Fracture Mechanics," ASTM 18th National Symposium on Fracture Mechanics, ASTM STP-945, 1986.

3. Kumar, V., German, M., and Shih, C. F., "An Engineering Approach for Elastic-Plastic Fracture Analysis," EPRI Report NP-1931 (R.P. 1237-1), Electric Power Research Institute, Palo Alto (CA), 1981.

4. Tada, H., Paris, P. C., and Irwin, G. R., "The Stress Analysis of Cracks Handbook," Second Edition, Paris Production, Inc. and Del Research Corp., St. Louis (MO), 1985.

TABLE 1: Thermo-Mechanical J_x-Integral Values for SEN Specimen Under Linear Temperature Gradient and Uniform Applied Stress

σ Appl = 65 ksi, L = 0.5 in, (a/w) = 0.25, (L/W) = 1.25

J_x-Integral Load Case #7	For Path 1 (lbs/in)	For Path 2 (lbs/in)	For Path 3 (lbs/in)	For Path 4 (lbs/in)	J_x-Average (lbs/in)
Rice	194.29	201.30	204.00	204.252	201.386
Ainsworth	136.58	138.12	138.10	138.27	137.793
Blackburn	163.50	163.46	163.50	164.25	163.678
Kishimoto	167.26	167.98	168.02	171.35	168.303
Atluri - T_p*	161.309	161.789	161.685	164.109	162.234
Atluri - T_p	308.179	308.644	308.5556	310.722	309.025
EPFM Handbook (1100F)	-	-	-	-	124.220

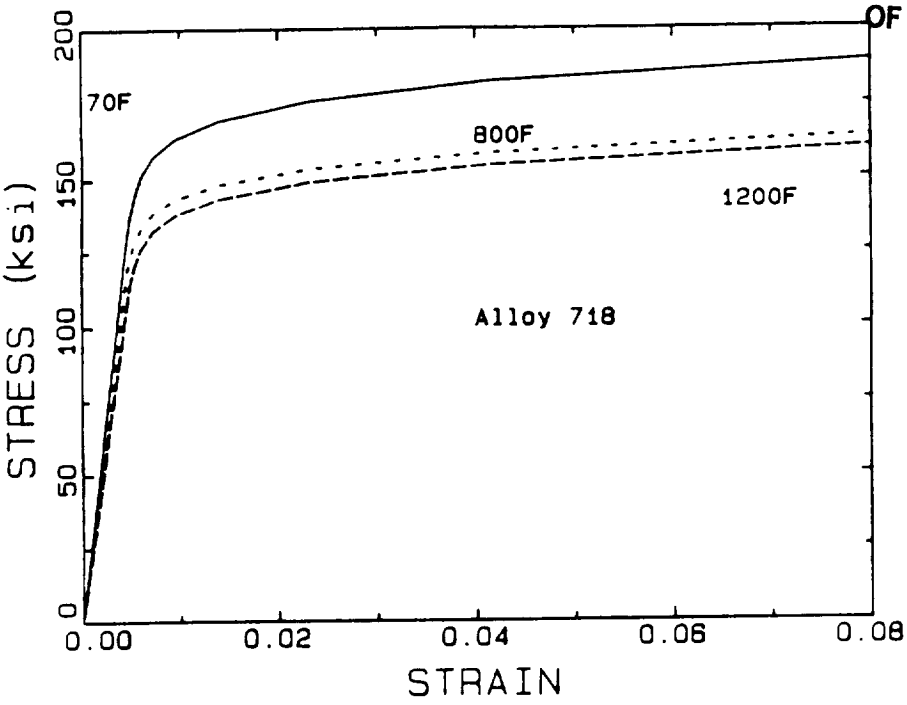

Figure 1: Tensile Curves for Alloy 718 at 70, 800 and 1200°F.

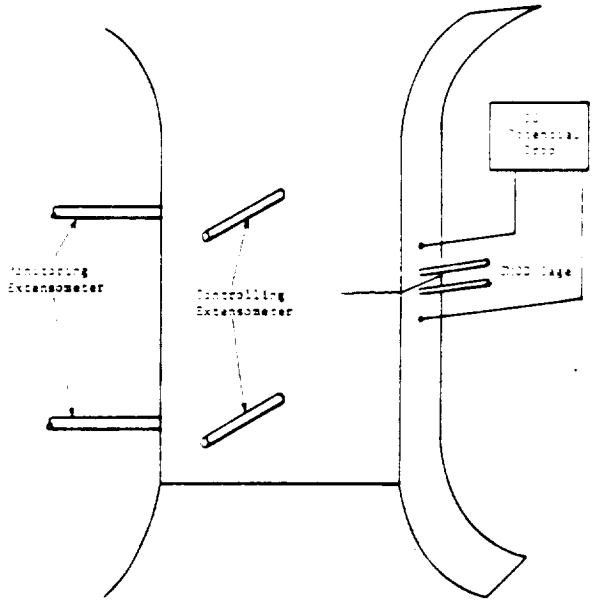

Figure 2: Schematic Drawing of SEN Specimen Test Method

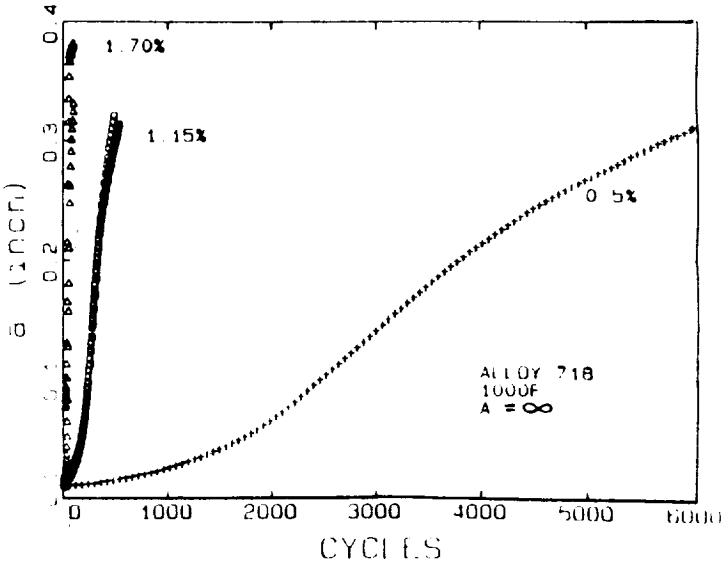

(a)

Results of 1000°F, Alloy 718

Displacement Control Tests

(a) crack depth versus cycles.

da/dN versus

(b) Δ K

(c) K_{max}.

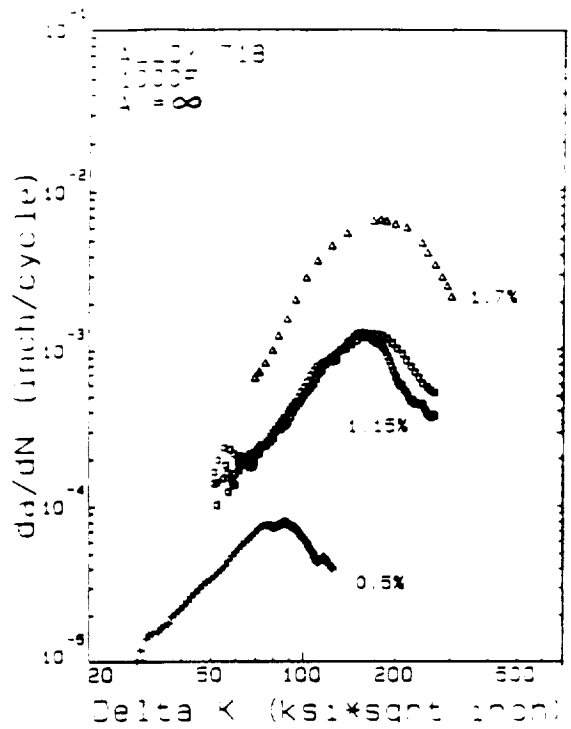

(b)

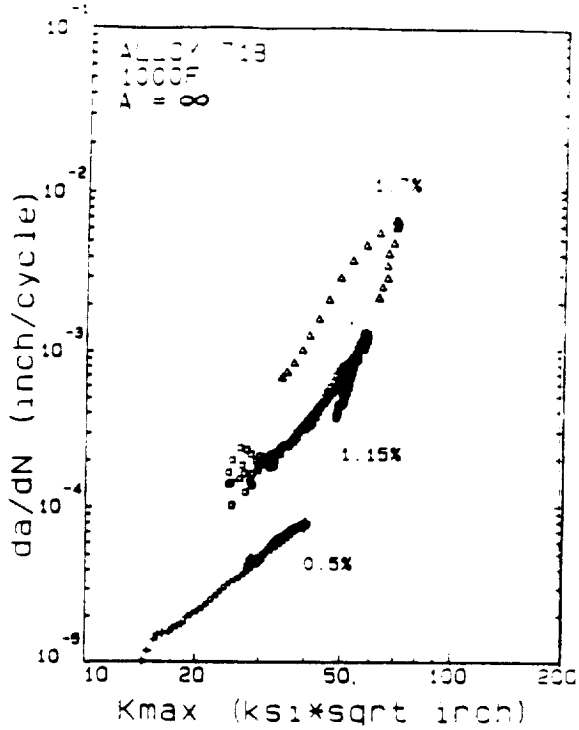

(c)

Figure 3

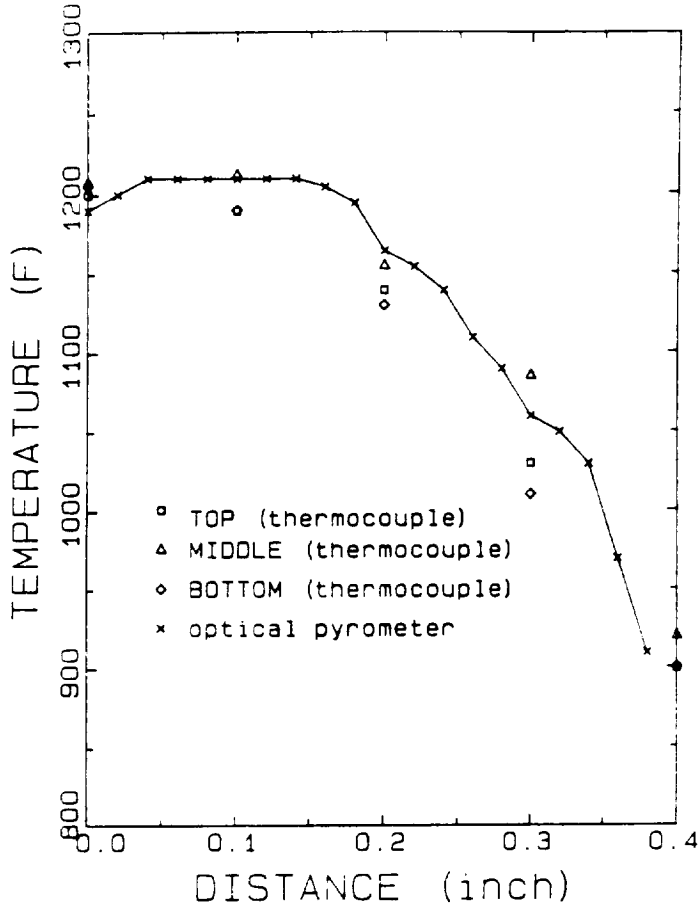

Figure 4: Temperature Profile in Thermal Gradient Tests

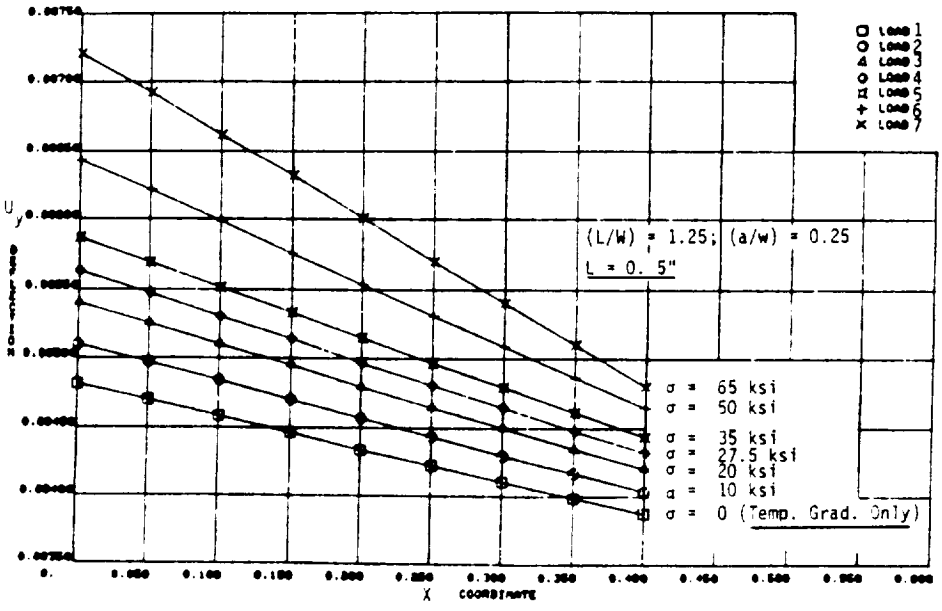

FIGURE 5: Far-Field U_y (y = 0.5") Displacement in SEN Specimen Under Linear Temperature Gradient and Applied Uniform Stress. (L/W = 1.25)

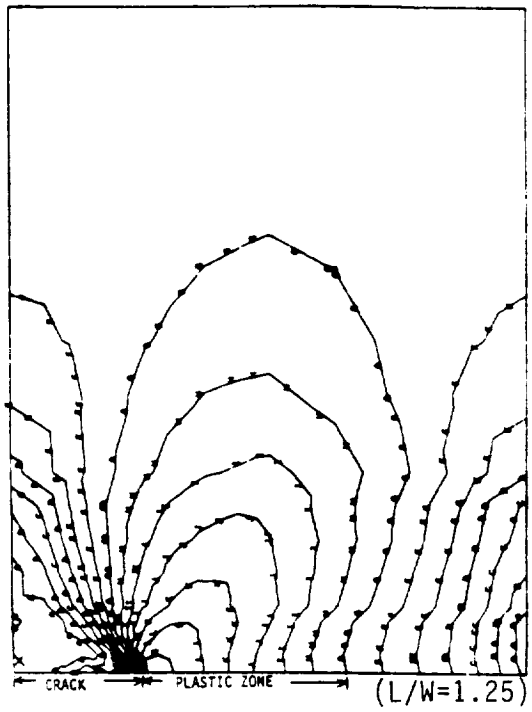

FIGURE 6: Effective Stress Contours in SEN Specimen Under Linear Temperature Gradient and Applied Stress of 65 ksi.

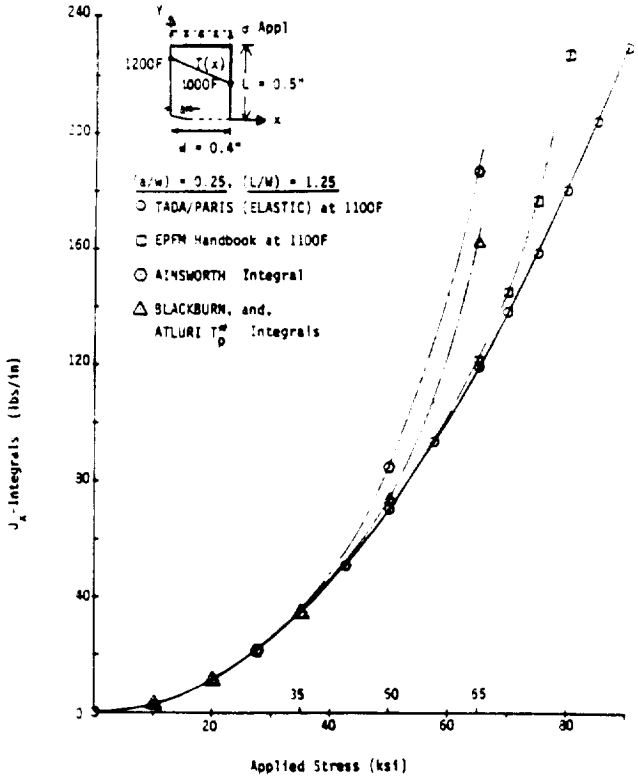

FIGURE 7: Thermo-Mechanical Elasto-Plastic J_k-Integrals in SEN Specimen Under Linear Thermal Gradient and Applied Uniform Far-Field Stress.

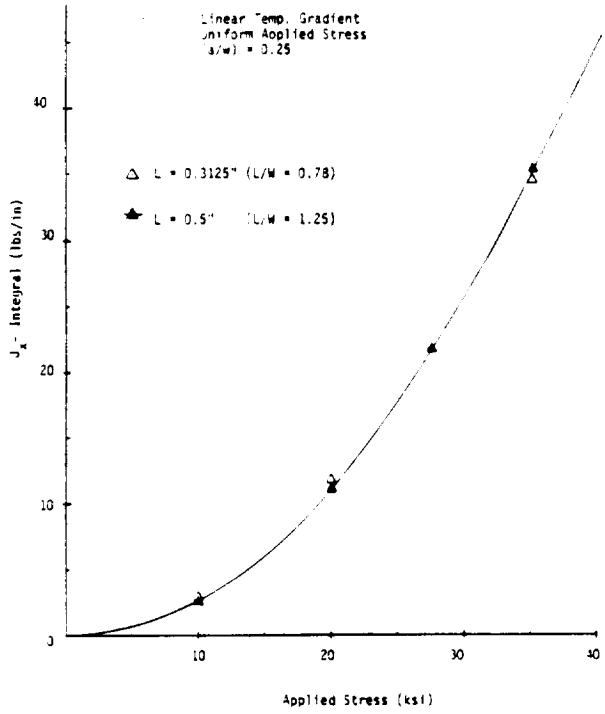

FIGURE 8: Thermo-Mechanical Kishimoto Integral in SEN Specimen

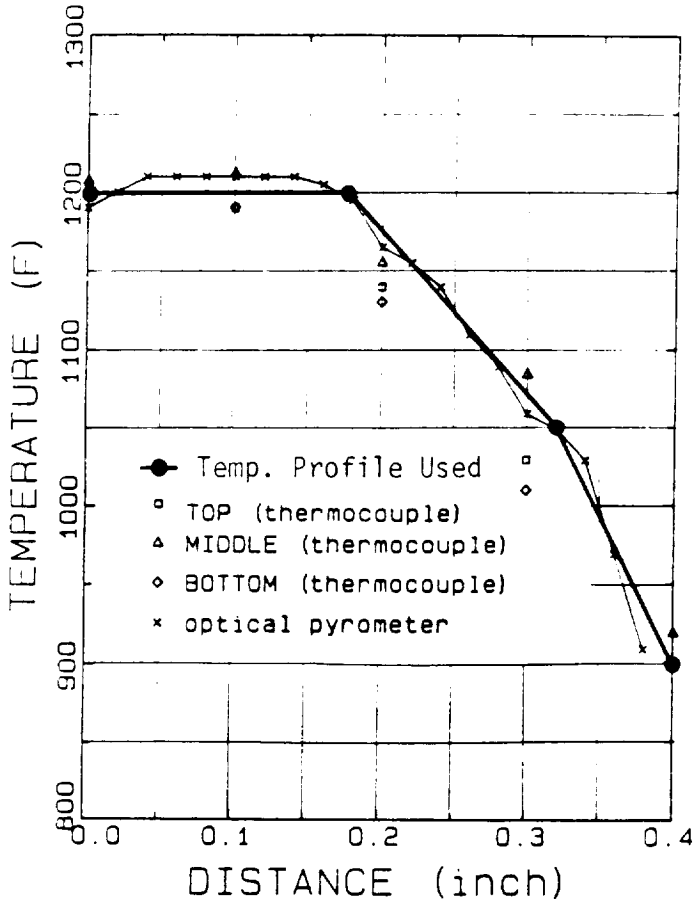

Figure 9: Trilinear Thermal Gradient Used in Analysis

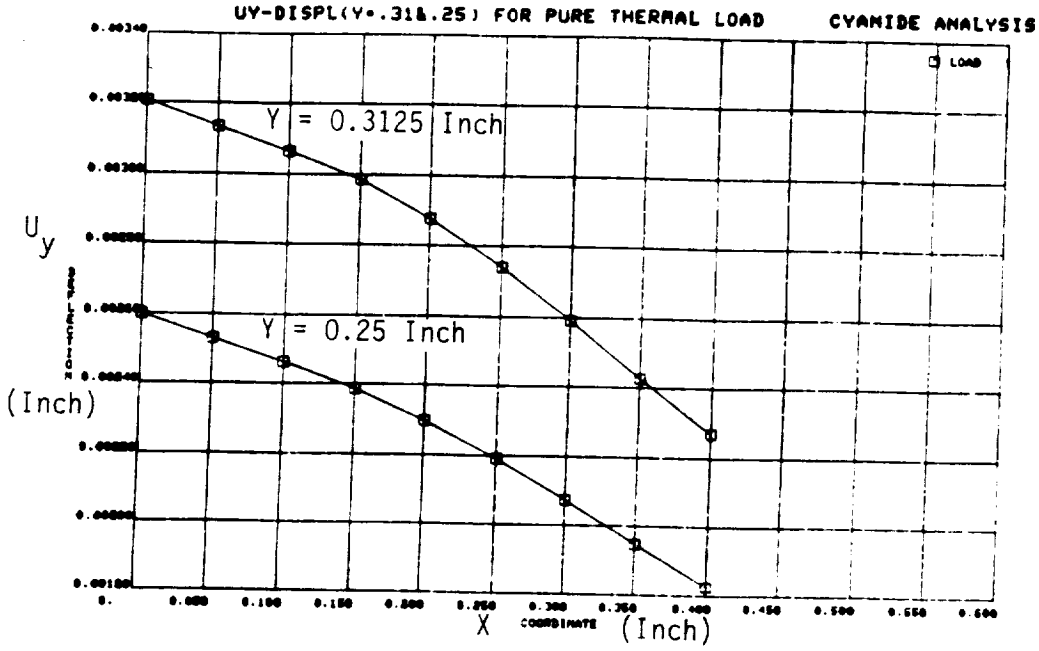

Figure 10: Far-Field Normal Displacement for Thermal Gradient

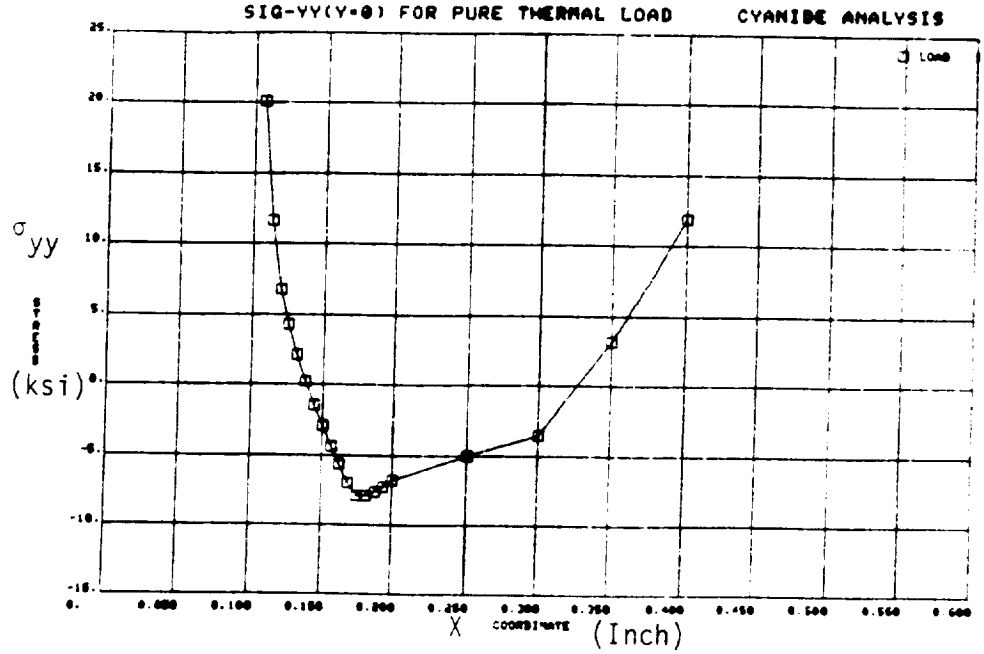

Figure 11: Normal Stress Ahead of Crack-Tip for Thermal Gradient

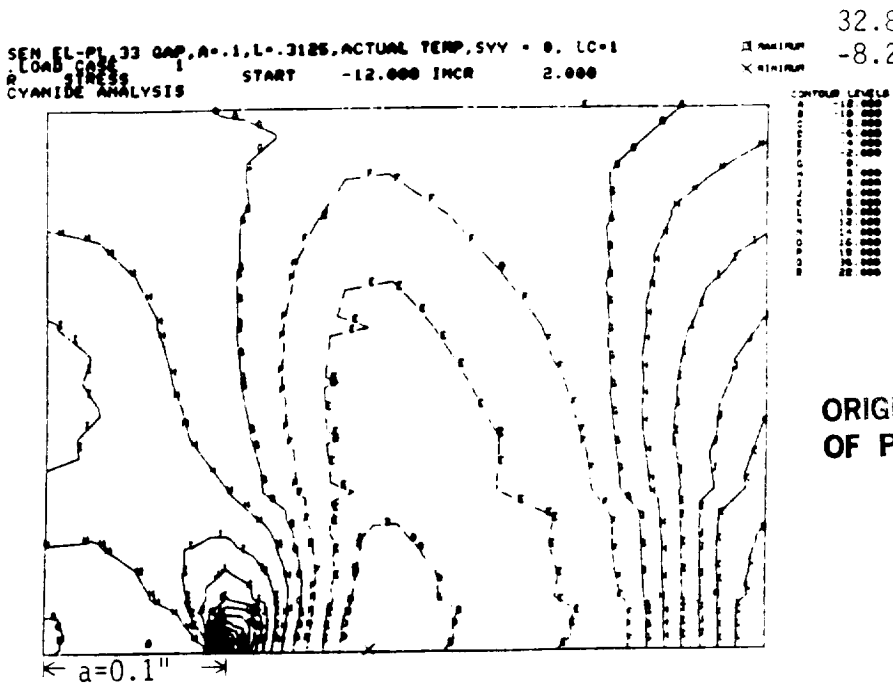

ORIGINAL PAGE IS
OF POOR QUALITY

Figure 12: Normal Stress (σ_{yy}) Contours for Thermal Gradient

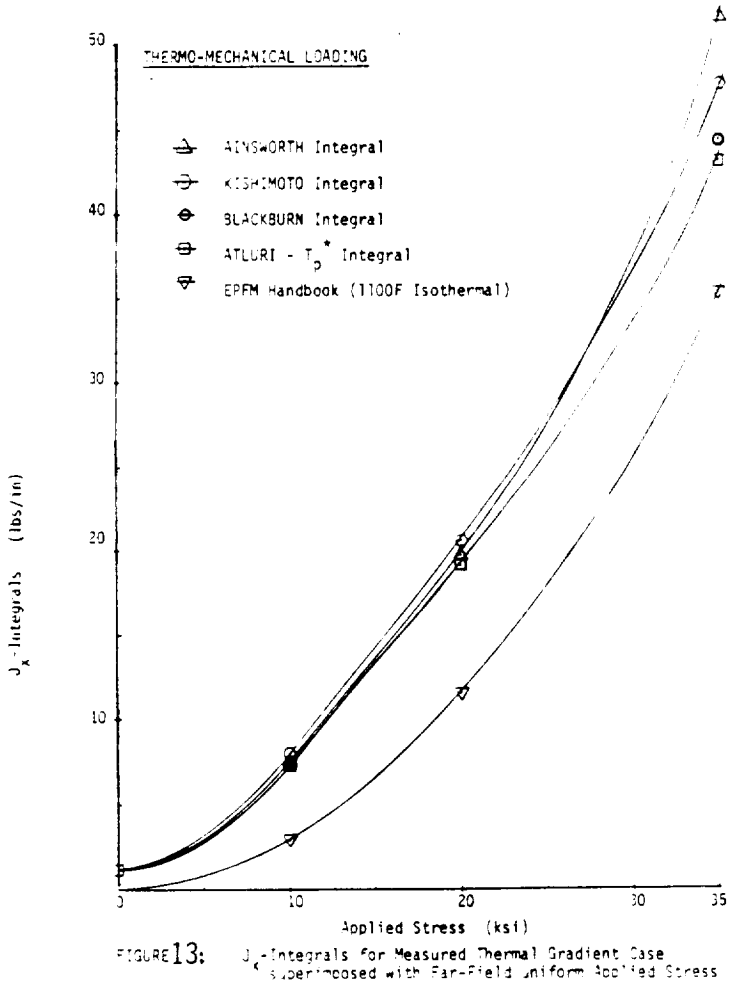

FIGURE 13: J_x-Integrals for Measured Thermal Gradient Case Superimposed with Far-Field Uniform Applied Stress